

Spin-Orbital Altermagnetism

Zi-Ming Wang^{1,2,*} Yang Zhang^{3,*†} Song-Bo Zhang^{4,5,‡} Jin-Hua Sun,⁶ Elbio Dagotto³
Dong-Hui Xu^{1,7,§} and Lun-Hui Hu^{2,3,||}

¹*Department of Physics and Chongqing Key Laboratory for Strongly Coupled Physics, Chongqing University, Chongqing 400044, China*

²*Center for Correlated Matter and School of Physics, Zhejiang University, Hangzhou 310058, China*


³*Department of Physics and Astronomy, University of Tennessee, Knoxville, Tennessee 37996, USA*

⁴*Hefei National Laboratory, Hefei, Anhui 230088, China*

⁵*International Center for Quantum Design of Functional Materials (ICQD), University of Science and Technology of China, Hefei, Anhui 230026, China*

⁶*Department of Physics, Ningbo University, Ningbo 315211, China*

⁷*Center of Quantum Materials and Devices, Chongqing University, Chongqing 400044, China*

 (Received 20 October 2024; revised 8 June 2025; accepted 4 August 2025; published 21 October 2025)

Altermagnetism is a newly discovered magnetic phase, characterized by nonrelativistic spin splitting that has been experimentally observed. Here, we introduce a framework dubbed “spin-orbital altermagnetism” to achieve spin-orbital textures in altermagnetic materials. We identify two distinct classes of spin-orbital altermagnetism: intrinsic and extrinsic. The intrinsic type emerges from symmetry-compensated magnetic orders with spontaneously broken parity-time symmetry, while the extrinsic type stems from translational symmetry breaking between sublattices, as exemplified by the Jahn-Teller-driven structural phase transition. In addition to directly measuring the spin-orbital texture, we propose spin conductivity and spin-resolved orbital polarization as effective methods for detecting these altermagnets. Additionally, a symmetry-breaking mechanism induces weak spin magnetization, further revealing the peculiar feature of spin-orbital altermagnetism. We also utilize the staggered susceptibility to illustrate a potential realization of this phase in a two-orbital interacting system. Our Letter provides a new platform to explore spin-orbital locked physics, extending the materials classes that may display complex spin textures from the standard $4d - 5d$ compounds to $3d$ compounds.

DOI: [10.1103/cjzw-j4v7](https://doi.org/10.1103/cjzw-j4v7)

Introduction—Spin and orbit are two fundamental degrees of freedom of electrons, and their intertwining is crucial for understanding various electronic states and phenomena in quantum materials [1]. Spin-orbit coupling (SOC), a relativistic effect in solids, couples these degrees of freedom, lifting the Kramers spin degeneracy and resulting in spin-split energy bands with distinctive spin textures in reciprocal space. Recent experiments using spin-resolved and photon-polarized angle-resolved photoemission spectroscopy [2] have revealed entangled spin-orbital textures—a locking phenomenon between spin and atomic orbital degrees of freedom—in strongly spin-orbit coupled systems such as topological insulators [3–5]. This breakthrough opens novel avenues for manipulating spin polarization by targeting the orbital domain.

Nonrelativistic mechanisms for spin-splitting effects have also garnered significant attention in recent years. These SOC-free phenomena have become prominent after the discovery of altermagnetism (AM) [6–16], which is a new magnetic phase characterized by momentum-dependent spin splitting despite zero net magnetization [17–20]. Subsequent experimental studies have confirmed AM-induced spin-splitting bands in diverse materials [21–32]. A few earlier theoretical works for nonrelativistic spin splitting were established through spin-channel Pomeranchuk instabilities [33–35] and d -wave spin-density wave states [36]. Furthermore, noncoplanar antiferromagnetic materials also exhibit significant nonrelativistic spin-split bands [37–44]. These novel magnetic systems can exhibit intriguing properties and potential functionalities [45–49].

Although distinct mechanisms for altermagnets have been proposed recently [50–58], other spin-related nonrelativistic phenomena, particularly the physics of spin-orbital textures without SOC, remain largely unexplored. This can be achieved through intertwined symmetry-compensated magnetic orders that couple these two degrees of freedom. Here, we establish a new theoretical framework to attain

*These authors contributed equally to this work.

†Contact author: yzhang@utk.edu

‡Contact author: songbozhang@ustc.edu.cn

§Contact author: donghuixu@cqu.edu.cn

||Contact author: lunhui@zju.edu.cn

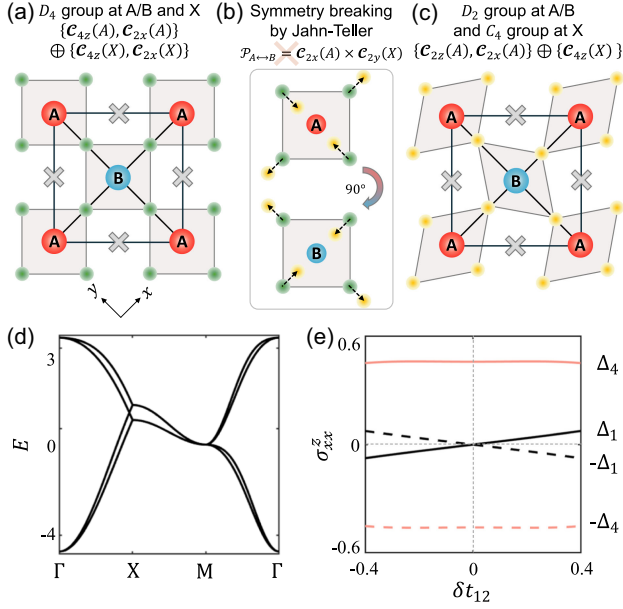


FIG. 1. (a) The square lattice with A (red) and B (blue) sublattices, each surrounded by four symmetric atoms (green). D_4 group at A/B and X $\{C_{4z}(A), C_{2x}(A)\} \oplus \{C_{4z}(X), C_{2x}(X)\}$. (b) Jahn-Teller distortions of green atoms around A and B , indicated by opposite-directional dot arrows. Symmetry breaking by Jahn-Teller $\mathcal{P}_{A \leftrightarrow B} = C_{2x}(A) \times C_{2y}(X)$. (c) The distorted lattice by combining (a) and (b). D_2 group at A/B and C_4 group at X $\{C_{2z}(A), C_{2x}(A)\} \oplus \{C_{4z}(X)\}$. (d) Tight-binding band structure for the lattice in (c). (e) Spin conductivity σ_{xx}^z as a function of JT distortion strength δt_{12} for \mathcal{O}_1 (JT-induced) and \mathcal{O}_4 (intrinsic) phases.

nonrelativistic spin-orbital textures through altermagnetic orders, dubbed “spin-orbit altermagnetism.” Among various altermagnetic orders permitted by spin-space symmetry [13], we identify two distinct classes of spin-orbit altermagnetism: one arising intrinsically and the other necessitating crystalline symmetry breaking due to structural phase transitions. We demonstrate that the spin conductivity and spin-resolved orbital polarization are effective tools for detecting and distinguishing between these phases. We also

examine the weak ferromagnetic magnetization caused by symmetry breaking, relevant to the hysteresis loop observed in the anomalous Hall effect. Furthermore, the staggered susceptibility is employed to illustrate a potential realization of such a phase in two-orbital interacting systems.

Intrinsic altermagnet—We study a square lattice with two sublattices, A and B , surrounded by a crystal field generated by four symmetrically positioned atoms, as shown in Fig. 1(a). If A is identical to B , the system exhibits the D_4 point group symmetry at both A and B sites and the centroid of the square (labeled “ X ” in gray). The symmetry generators are $\{C_{4z}(A), C_{2x}(A)\}$ and $\{C_{4z}(X), C_{2x}(X)\}$, leading to three symmetries that relate A to B : (i) fourfold rotation $C_{4z}(X)$, (ii) inversion $\mathcal{P}_{A \leftrightarrow B} = C_{2x}(A)C_{2y}(X)$, and (iii) mirror $\mathcal{M}_{A \leftrightarrow B} = C_{4z}(X)C_{2x}(A)$. In this case, the symmetry-compensated magnetic order arises from breaking time-reversal symmetry \mathcal{T} while preserving at least one of the following spin-space group symmetries: $[C_2 || \mathcal{P}_{A \leftrightarrow B}]$, $[C_2 || C_{4z}(X)]$, and $[C_2 || \mathcal{M}_{A \leftrightarrow B}]$ [59]. Here, the left element C_2 acts solely on spin space (i.e., flipping spins), while the right elements act purely in real space. Since SOC is absent or negligible, the spin-space group provides a comprehensive framework for classifying collinear magnetic orders [13] and others [60]. Furthermore, in a two-orbital system, two additional symmetries, $[C_2 || C_{4z}(A)]$ and $[C_2 || C_{2x}(A)]$, permit a staggered magnetic order between the two orbitals. Thus, based on spin-space symmetry analysis [see Sec. I of Supplementary Material (SM) [61]], five staggered orders are identified in Table I. These orders all feature zero net magnetization and are generally classified as antiferromagnetic or altermagnetic. Their matrix representations $\mathcal{O}_{1 \rightarrow 5}$ are $\{\tau_0 \sigma_z s_z, \tau_x \sigma_z s_z, \tau_x \sigma_0 s_z, \tau_z \sigma_0 s_z, \tau_z \sigma_z s_z\}$, where τ , σ , and s denote Pauli matrices for orbital, sublattice, and spin degrees of freedom, respectively.

We now discuss general results in Table I with $\mathcal{P}_{A \leftrightarrow B}$. Collinear antiferromagnets can be either Néel or altermagnetic types [13]. The \mathcal{O}_1 phase represents the Néel order, which preserves $\mathcal{P}_{A \leftrightarrow B} \mathcal{T}$, similar to \mathcal{O}_2 and \mathcal{O}_5 . According to Kramers theorem, bands in these phases maintain spin degeneracy. However, \mathcal{O}_3 and \mathcal{O}_4 violate $\mathcal{P}_{A \leftrightarrow B} \mathcal{T}$ spontaneously, qualifying them as intrinsic altermagnets. They both

TABLE I. Symmetry classification and properties of five staggered orders, with or without inversion ($\mathcal{P}_{A \leftrightarrow B}$), in a two-orbital square-lattice system with sublattices A and B . The spin-space group operator g acts on \mathcal{O}_i as follows: $g[\mathcal{O}_i]g^\dagger = \chi_i \mathcal{O}_i$, where the character $\chi_i = \pm 1$ corresponds to the symbols \checkmark and \times , respectively. Here, AM, AFM, FM, and SO denote altermagnetism, antiferromagnetic, ferromagnetism, and spin-orbital, respectively. g -wave is planar type.

AFM order	$\mathcal{P}_{A \leftrightarrow B}$	Symmetry					With $\mathcal{P}_{A \leftrightarrow B}$	w/o $\mathcal{P}_{A \leftrightarrow B}$
		$\{C_2 \mathcal{P}_{A \leftrightarrow B}\}$	$C_{4z}(X)$	$\{C_2 C_{4z}(X)\}$	$\mathcal{M}_{A \leftrightarrow B}$	$\{C_2 \mathcal{M}_{A \leftrightarrow B}\}$		
$\mathcal{O}_1: \tau_0 \sigma_z s_z$	\times	\checkmark	\times	\checkmark	\times	\checkmark	d -wave AM $\sigma_{xx}^z \neq 0$	
$\mathcal{O}_2: \tau_x \sigma_z s_z$	\times	\checkmark	\checkmark	\times	\times	\checkmark	Néel AFM $\sigma_{\mu\nu}^z = 0$ SO g -wave AM $\sigma_{\mu\nu}^z = 0$	
$\mathcal{O}_5: \tau_z \sigma_z s_z$	\times	\checkmark	\checkmark	\times	\checkmark	\times	Weak FM	
$\mathcal{O}_3: \tau_x \sigma_0 s_z$	\checkmark	\times	\times	\checkmark	\times	\checkmark	Intrinsic SO d -wave AM $\sigma_{xy}^z = \sigma_{yx}^z \neq 0$	
$\mathcal{O}_4: \tau_z \sigma_0 s_z$	\checkmark	\times	\times	\checkmark	\checkmark	\times	Intrinsic SO d -wave AM $\sigma_{xx}^z = -\sigma_{yy}^z \neq 0$	

feature d -wave altermagnetism, with subtle differences. For \mathcal{O}_3 , it adheres to $[\mathcal{C}_2|\mathcal{C}_{2x}(A)]$, which enforces the band constraint $[\mathcal{C}_2|\mathcal{C}_{2x}(A)]\epsilon_n(s, k_x, k_y) = \epsilon_n(-s, k_x, -k_y)$, leading to nodal lines along $k_x = 0$ or $k_y = 0$. In contrast, the \mathcal{O}_4 phase shows $[\mathcal{C}_2|\mathcal{M}_{A\leftrightarrow B}]$ -protected nodal lines along $k_x = \pm k_y$.

Extrinsic altermagnet—In addition to $\mathcal{O}_{3/4}$, other symmetry-compensated orders can transition into altermagnets via symmetry breaking. Here, we examine crystalline symmetry breaking induced by the Jahn-Teller (JT) mode [Fig. 1(b)]. In this case, the directions of lattice distortions for the A and B sublattices are opposite, resulting in a different crystal field environment compared to the symmetric case [Fig. 1(a)]. As shown in Fig. 1(c), the symmetry of the distorted lattice reduces to the D_2 group at A/B ($\{\mathcal{C}_{2z}(A), \mathcal{C}_{2x}(A)\}$) and the C_4 group at X ($\{\mathcal{C}_{4z}(X)\}$). Specifically, the JT mode breaks the $\mathcal{P}_{A\leftrightarrow B}$ symmetry or equivalently $C_{2y}(X)$.

Table I summarizes the effects of breaking $\mathcal{P}_{A\leftrightarrow B}$ symmetry while preserving other symmetries. Here we focus on the extrinsic spin-splitting bands in phases $\mathcal{O}_{1/2/5}$. By symmetry, \mathcal{O}_1 belongs to a d -wave altermagnet with nodal lines along $k_x = \pm k_y$. \mathcal{O}_2 represent planar g -wave spin-orbital AM, displaying four nodal lines along $k_x = 0$, $k_y = 0$, and $k_x = \pm k_y$. As expected, \mathcal{O}_5 breaks all the symmetries required to classify it as an antiferromagnetic phase, so that it exhibits a nonzero net spin magnetization.

To quantitatively investigate the influence of the JT mode, we employ a tight-binding model within the mean-field (MF) formalism for the staggered orders,

$$\begin{aligned} \mathcal{H}_{\text{MF}}(\mathbf{k}) = & \mathcal{H}_0(\mathbf{k})s_0 + \Delta_1\tau_0\sigma_zs_z + \Delta_2\tau_x\sigma_zs_z \\ & + \Delta_3\tau_x\sigma_0s_z + \Delta_4\tau_z\sigma_0s_z + \Delta_5\tau_z\sigma_zs_z, \end{aligned} \quad (1)$$

where Δ_i with $i \in \{1, \dots, 5\}$ are order parameters corresponding to the \mathcal{O}_i orders, and we assume that s_z is conserved. The noninteracting part is $\mathcal{H}_0(\mathbf{k}) = \tau_0[\epsilon_0(\mathbf{k})\sigma_0 + \epsilon_1(\mathbf{k})\sigma_x + \epsilon_3(\mathbf{k})\sigma_z] + [f_1(\mathbf{k})\tau_x + f_3(\mathbf{k})\tau_z]\sigma_0$ with $\epsilon_0(\mathbf{k}) = -(t_1 + t_2)(\cos 2k_x + \cos 2k_y)$, $\epsilon_1(\mathbf{k}) = -2t_0(\cos k_x + \cos k_y)$, $\epsilon_3(\mathbf{k}) = (t_2 - t_1)(\cos 2k_x - \cos 2k_y)$, $f_1(\mathbf{k}) = -4t_3 \sin k_x \sin k_y$, and $f_3(\mathbf{k}) = 2t_5(\cos 2k_x - \cos 2k_y)$. Cartoon representations of these hoppings are illustrated in Sec. I of SM [61]. We consider the intersublattice hopping t_0 as the dominant energy scale, which has been demonstrated to support the metallic altermagnetic phase [62]. Moreover, we define $\delta t_{12} \equiv (t_1 - t_2)/(t_1 + t_2)$ as a measure of the lattice distortion while disregarding other factors. The band structure for the distorted lattice is presented in Fig. 1(d), using the parameters $t_0 = 1$, $t_3 = 0.07$, $t_5 = 0.04$, $t_1 = 0.2$, and $t_2 = 0.1$ (i.e., $\delta t_{12} = 1/3$). In our JT-induced extrinsic altermagnetism, $\delta t_{12} \neq 0$ resembles the effects of lattice strain effect and ferroelectricity [54–58], both of which also break $\mathcal{P}_{A\leftrightarrow B}$.

The JT-induced altermagnetic phases can be detected via spin-conductivity measurements [72–74]. The spin current carries spin polarization along the z direction, given by $J_\mu^z = \sigma_{\mu\nu}^z E_\nu$ with $\mu, \nu \in \{x, y\}$. Symmetry constraints dictate that the nonzero components are $\sigma_{xx}^z = -\sigma_{yy}^z \neq 0$ for \mathcal{O}_1 and \mathcal{O}_4 , $\sigma_{xy}^z = \sigma_{yx}^z \neq 0$ for \mathcal{O}_3 , whereas all components vanish for \mathcal{O}_2 . We calculate explicitly $\sigma_{\mu\nu}^z$ as a function of δt_{12} for \mathcal{O}_1 (extrinsic altermagnet) and \mathcal{O}_4 (intrinsic altermagnet), employing the linear response theory [75]. The results are shown in Fig. 1(e). σ_{xx}^z changes sign upon reversing Δ_1 or Δ_4 . Below the Néel temperature ($T < T_N$), the system can exhibit d -wave or g -wave AM, following a structural phase transition ($T < T_S$). In the d -wave scenario, if $T_N > T_S$, $\sigma_{xx}^z \neq 0$ in the \mathcal{O}_1 phase only when $T < T_S$. Thus, spin conductivity can be a new means to detect the JT mode, serving as an alternative to scanning transmission electron microscopy [76]. While σ_{xx}^z is small for \mathcal{O}_1 at small δt_{12} , it can be enhanced by tuning μ or considering JT-induced crystal fields (see Sec. II of SM [61]). Notably, σ_{xx}^z of extrinsic altermagnets undergoes a sign change when the sign of δt_{12} is inverted, whereas this behavior is absent in intrinsic altermagnets.

Spin-orbital texture—To understand the underlying difference among \mathcal{O}_1 , \mathcal{O}_4 , and the other phases, we introduce the spin-orbital weight or texture. In Sec. III of SM [61], we derive the effective mean-field $\mathbf{k} \cdot \mathbf{p}$ Hamiltonian around the Γ (or M) point for Eq. (1). By projecting out the sublattice degrees of freedom, we obtain

$$\begin{aligned} \mathcal{H}_\Gamma(\mathbf{k}) = & E_0(\mathbf{k}) - [4t_3k_xk_y\tau_x + 4t_5(k_x^2 - k_y^2)\tau_z]s_0 \\ & + [\tilde{\Delta}_1(\mathbf{k})\tau_0 + \tilde{\Delta}_2(\mathbf{k})\tau_x + \Delta_3\tau_x + \Delta_4\tau_z]s_z, \end{aligned} \quad (2)$$

where $E_0(\mathbf{k}) = m_0(k_x^2 + k_y^2)$ with $m_0 = 2(t_1 + t_2) - t_0$, $J = (t_1 - t_2)/(2t_0) \propto \delta t_{12}$, $\tilde{\Delta}_1(\mathbf{k}) = J\Delta_1(k_x^2 - k_y^2)$, and $\tilde{\Delta}_2(\mathbf{k}) = J\Delta_2(k_x^2 - k_y^2)$. This shows the differences between the JT-induced and intrinsic altermagnets. While the term $\tilde{\Delta}_{1/2}$ is induced by the JT mode, $\Delta_{3/4}$ represent intrinsic altermagnets. The spin splitting is elucidated from commutation relations, e.g., $[\epsilon_3(\mathbf{k})\tau_0\sigma_zs_0, \Delta_1\tau_0\sigma_zs_z] = 0$. This implies that changing the sign of δt_{12} is analogous to flipping the sign of Δ_1 , which accounts for the observed sign reversal in σ_{xx}^z . Moreover, the spin-split Fermi surfaces for each altermagnetic phase are illustrated in Figs. 2(a)–2(d), respectively. Specifically, Fig. 2(b) illustrates the g -wave character, while Figs. 2(a), 2(c), and 2(d) show the d -wave altermagnets, in agreement with our symmetry analysis.

Remarkably, all altermagnetic phases except for \mathcal{O}_1 display orbital dependencies, showcasing nontrivial spin-orbital textures. To illustrate this, we first define the spin-resolved orbital weight on each Fermi surface,

$$p_s^n(\theta_k) = \langle E_{n,s}(k_{f,s}^{(n)}, \theta_k) | \tau_z | E_{n,s}(k_{f,s}^{(n)}, \theta_k) \rangle, \quad (3)$$

where $|E_{n,s}(k, \theta_k)\rangle$ represents the eigenstate of $\mathcal{H}_\Gamma(k, \theta_k)$ in

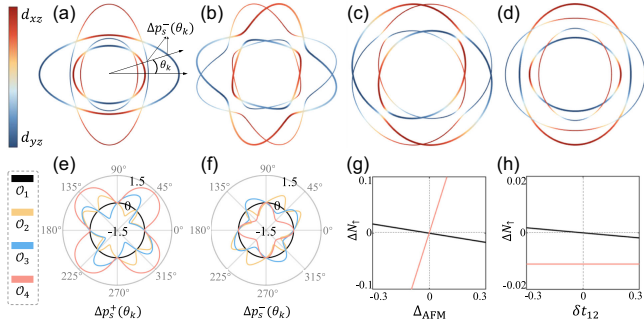


FIG. 2. (a)–(d) Spin-split Fermi surfaces for $\mathcal{O}_{1/2/3/4}$, respectively, with the thick (thin) lines denoting the $s_z = \uparrow$ (\downarrow) bands. The color scheme represents the orbital weight on the Fermi surfaces. (e), (f) Corresponding spin-orbital textures $\Delta p_s^\pm(\theta_k)$ for the $+$ (inner Fermi surfaces) and $-$ bands (outer Fermi surfaces), respectively, as illustrated in (a). (g), (h) Spin-resolved orbital polarization as a function of the altermagnetic gap $\Delta_{\text{AFM}} = \Delta_1$ (black) and $\Delta_{\text{AFM}} = \Delta_4$ (red), and JT distortion strength δt_{12} , respectively. Parameters for the $\mathbf{k} \cdot \mathbf{p}$ model are derived from the tight-binding model used in Fig. 1(d), with $m_0 = -0.2$ for better visualization. Other parameters are $\mu = 2.5$, $\Delta_1 = 2.5$, $\Delta_2 = 3.5$, and $\Delta_{3/4} = 0.2$.

polar coordinates, $n = \pm$ is the band index without spin-splittings ($\Delta_i = 0$), $s = \{\uparrow, \downarrow\}$ denotes spin, and $k_{f,s}^{(n)}$ is the associated Fermi momentum. We present the main results in Figs. 2(e) and 2(f) and provide the analytical expressions in Sec. IV of SM [61]. Then, we introduce

$$\Delta p_s^n(\theta_k) = p_\uparrow^n(\theta_k) - p_\downarrow^n(\theta_k), \quad (4)$$

to capture the spin-orbital texture of the n th band. We show $\Delta p_s^+(\theta_k)$ in Fig. 2(e) and $\Delta p_s^-(\theta_k)$ in Fig. 2(f). Unlike the other phases, Δp_s^\pm only vanishes in the \mathcal{O}_1 phase [77]. Thus, $\Delta p_s \neq 0$ signifies spin-orbital textures and characterizes spin-orbital AM, which features a spin-orbital-locked magnetic ordering. Moreover, Δp_s varies significantly among different phases due to their distinct symmetry characteristics, i.e., $\Delta p_s^n(\theta_k) = \Delta p_s^n[(\pi/2) - \theta_k] = -\Delta p_s^n[(\pi/2) + \theta_k]$ for \mathcal{O}_2 , $\Delta p_s^n(\theta_k) = -\Delta p_s^n[(\pi/2) - \theta_k]$ for \mathcal{O}_3 , and $\Delta p_s^n(\theta_k) = \Delta p_s^n[(\pi/2) - \theta_k]$ for \mathcal{O}_4 .

Furthermore, the spin-resolved and angle-dependent intensity is defined as

$$\mathcal{I}_s(\theta_k) = \int_0^\infty k dk \sum_n \delta(E_f - E_{n,s}(k, \theta_k)) p_s^n(\theta_k), \quad (5)$$

where $\delta(x)$ is the delta function. The total spin-resolved intensity is then obtained as $\mathcal{N}_s = \int_0^{2\pi} \mathcal{I}_s(\theta_k) d\theta_k$. It measures the orbital polarization $\mathcal{N}_s = N_{s,d_{xz}} - N_{s,d_{yz}}$, where $N_{s,d_{xz}}$ ($N_{s,d_{yz}}$) denotes spin-resolved density of states in the d_{xz} (d_{yz}) orbital. In Figs. 2(g) and 2(h), we plot $\Delta \mathcal{N}_s = |\mathcal{N}_s / (N_{s,d_{xz}} + N_{s,d_{yz}})|$ as a function of Δ_i and δt_{12} ,

respectively. Interestingly, $\Delta \mathcal{N}_s$ is nonzero for both \mathcal{O}_1 and \mathcal{O}_4 , whereas it vanishes for others. This distinction arises from the sign-changing behavior of p_s^n for the $\mathcal{O}_{\text{AFM},2/3}$ phases. The dependence on δt_{12} can be also used to distinguish \mathcal{O}_1 (JT-induced extrinsic altermagnet) from \mathcal{O}_4 (intrinsic altermagnet), particularly for $T_N < T_S$.

Effect of JT-induced crystal field—The \mathcal{O}_1 phase lacks a spin-orbital texture. However, this changes when considering a \mathcal{Q}_2 JT mode. As derived in Sec. V of SM [61], this JT mode introduces both δt_{12} and a staggered crystal field, represented as $\delta_{\text{JT}} \tau_z \sigma_z$. When $\delta_{\text{JT}} > J\Delta_1$, a second-order perturbation yields an additional term $\delta_{\text{JT}} \Delta_1 / (4t_0) \tau_z s_z$ in Eq. (2). This term effectively resembles that of the \mathcal{O}_4 phase, as both phases share the same symmetry classification when $\delta t_{12} \neq 0$. Therefore, the interplay between δ_{JT} and \mathcal{O}_1 significantly intensify $\Delta p_s^n(\theta_k)$, which is proportional to δ_{JT} . We note that δ_{JT} can reach substantial magnitudes (e.g., 0.5 eV as reported in Ref. [63]), rendering the \mathcal{O}_1 -induced $\Delta p_s^n(\theta_k)$ comparable in magnitude to that from the \mathcal{O}_2 phase. We also explore this mechanism for spin-orbital textures in candidate materials (see Sec. V of SM [61]). Therefore, we conclude that spin-orbital texture is a universal feature of both intrinsic and extrinsic altermagnets.

Weak magnetization—The spin-orbital texture for the \mathcal{O}_5 phase are provided in Sec. VII of SM [61]. Below, we discuss two general mechanisms for generating magnetization in altermagnets. The first mechanism arises from the breaking of crystalline symmetries such as $\mathcal{P}_{A \leftrightarrow B}$ and $\mathcal{M}_{A \leftrightarrow B}$. Lifting symmetry constraints result in the effective local moments at the two sublattices becoming nonequivalent, leading to ferrimagnetism [Fig. 3(a)]. We calculate the

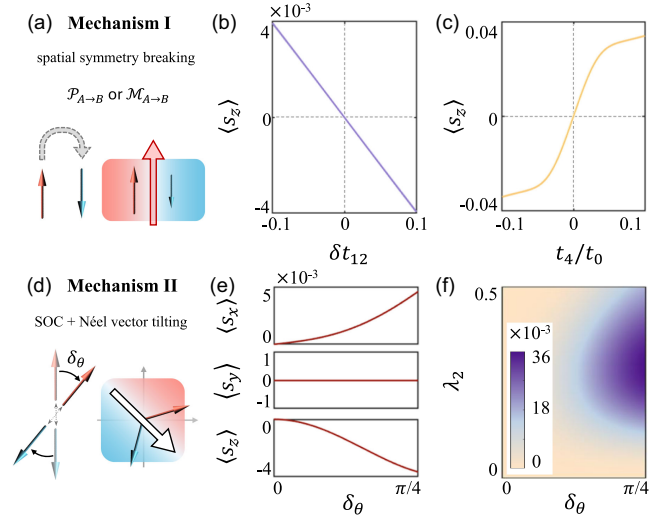


FIG. 3. (a) Illustration of weak magnetization (ferrimagnetism) resulting from the breaking of crystalline symmetries in an altermagnet. The calculated $\langle s_z \rangle$ are presented in (b) for \mathcal{O}_5 and in (c) for \mathcal{O}_2 , respectively. (d) Depiction of noncollinear magnetic order generated by SOC, effectively tilting the Néel vector. Calculations of $\langle \vec{s} \rangle$ for \mathcal{O}_1 are shown in (e) and (f). Parameters are the same as those used in Fig. 1(d).

magnetization $\langle s_z \rangle$ for \mathcal{O}_5 as a function of δt_{12} [Fig. 3(b)] [78]. Additionally, an example of $\mathcal{M}_{A \leftrightarrow B}$ -breaking terms, such as $-2t_4(\cos k_x - \cos k_y)\tau_y\sigma_y s_0$, can induce magnetization in the \mathcal{O}_2 phase [Fig. 3(c)]. In both cases, the system retains $[\mathcal{C}_2 | \mathcal{C}_{4z}(X)]$, restricting magnetization to align along the Néel-vector direction.

The second mechanism, applicable to both extrinsic and intrinsic altermagnets, involves SOC. It gives rise to a noncollinear magnetic order that consequently generates Berry curvature. In practice, we tilt the Néel vector from the z axis to an arbitrary direction (e.g., the x axis), such that the fourfold rotation couples spatial rotation with internal spin rotation. Thus, the $[\mathcal{C}_2 | \mathcal{C}_{4z}]$ symmetry is broken, as illustrated in Fig. 3(d). The effective polarization angles of the local moments at the two sublattices become misaligned, giving rise to magnetization that plays a role akin to the Dzyaloshinskii-Moriya interaction [79,80], as numerically confirmed in Fig. 3(e). For the calculations, $\mathcal{H}_{\text{SOC}} = \lambda_1 \tau_y \sigma_0 s_z + \lambda_2 \tau_0 \sigma_z (\sin 2k_x s_y - \sin 2k_y s_x)$ is used, where λ_1 is the atomic SOC and λ_2 is the $\mathcal{P}_{A \leftrightarrow B}$ -preserving Rashba SOC. We take the \mathcal{O}_1 phase for example and calculate the magnetization as a function of λ_2 and tilting angle δ_θ in Fig. 3(f). The magnetization intensifies with increasing λ_2 and δ_θ . This further generates a hysteresis loop in the anomalous Hall effect [23], with calculations provided in Sec. VI of SM [61].

Possible realization—Finally, we explore a potential realization of spin-orbital altermagnets using a mean-field approach and then calculate the staggered susceptibility, $\chi_i(T) = -[(k_B T)/2] \sum_{i\omega_n, \mathbf{k}} \text{Tr}[G_0(i\omega_n, \mathbf{k}) \mathcal{O}_i G_0(i\omega_n, \mathbf{k}) \mathcal{O}_i]$, where T , ω_n , and G_0 are the temperature, Matsubara frequency, and noninteracting Green's function, respectively (see Sec. VIII of SM [61]). The dominant contribution to χ_i arises from interband parts, and it converges to a finite value as T approaches zero [64]. Using the same parameters as in Fig. 1(d), we plot the maximum value of $\chi_i(T)$ as a function of chemical potential μ near the half filling, and find that the JT-induced altermagnets ($\mathcal{O}_{1/2}$) are predominant [Fig. 4(a)]. Upon setting $t_5 = 0$, one can analytically show $\chi_1 = \chi_2$ for the model in Eq. (1) (see Sec. VIII of SM [61]). However, our numerical results show

that χ_2 becomes dominant when $t_5 \neq 0$ [Fig. 4(b)]. This can be understood in the context of half filling. For \mathcal{O}_1 , the t_5 term is inactive in mediating electron hopping within the same sublattice. Whereas, \mathcal{O}_2 permits such hopping, thereby lowering the system's energy.

We confirm that the momentum-resolved bare susceptibilities $\xi_i(\mathbf{q})$ exhibit a pronounced peak at the Γ point in Sec. IX of SM [61]. Therefore, we can calculate the Néel temperature by solving the linearized gap equation, $\chi_i(T_N) = 1/U_i$, where U_i represents the effective interaction in \mathcal{O}_i . The absence of divergence in χ_i suggests a finite critical interaction to stabilize altermagnets, in agreement with self-consistent calculations. Based on the two-orbital $U - U' - J_H$ Hubbard model, the effective interactions are $U_1 = U + J_H$ for \mathcal{O}_1 and $U_2 = U - J_H$ for \mathcal{O}_2 . Thus, U_1 is always larger than U_2 as Hund's rule requires. This indicates that \mathcal{O}_2 is likely the leading phase at smaller J_H but larger t_5 , giving rise to the spin-orbital altermagnet, as illustrated in the $U - J_H$ phase diagram [Fig. 4(c)]. This is further supported by calculating random-phase-approximation renormalized susceptibilities [81]. Furthermore, the interaction-driven phase transition from a planar g -wave to d -wave altermagnet differs from previous reports [48,52,54]. Our theoretical framework for spin-orbital altermagnetism can be generalized to investigate phase transitions between distinct magnetic orders.

Conclusion—In summary, we show the crucial role of AM phases in achieving nonrelativistic spin-orbital texture by considering the intertwined orderings between spin and orbital degrees of freedom. We demonstrate that both extrinsic (e.g., JT-induced) and intrinsic altermagnets can host nontrivial spin-orbital textures with distinct characteristics. These altermagnetic phases can be detected via spin conductivity and spin-resolved orbital polarization for a two-orbital interacting model. We also discuss potential realizations for spin-orbital altermagnets based on the Ginzburg-Landau theory. Additionally, weak magnetization induced by symmetry breaking, with or without SOC, can occur in the altermagnets. Our results suggest that other structural phase transitions beyond JT distortions can also lead to the crossover from a Néel antiferromagnet to an altermagnet. Thus, our Letter can guide future experiments on searching materials and observing those intriguing states, particularly in square-planar systems with d^1 or d^2 high-spin and $3d$ low-spin states, as well as in octahedral systems with d^1 or d^2 high-spin and d^3 or d^4 low-spin states. The spin-momentum orbital locking in spin-orbital altermagnets may enable efficient electrical magnetization control by spin-orbit torques.

Note added—We recently became aware of several preprints addressing related phenomena, including spin-orbital locking effects in extrinsic altermagnets (\mathcal{O}_1) [82], and candidate materials for intrinsic altermagnetism (\mathcal{O}_4) [83,84].

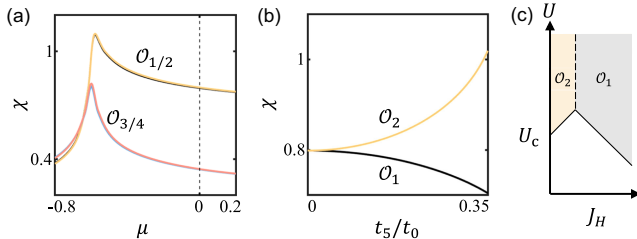


FIG. 4. (a) Maximal value of $\chi_i(T)$ as a function of the chemical potential μ for $\mathcal{O}_{1/2/3/4}$, with the dashed line marking the half filling. (b) χ_1 and χ_2 (the two leading phases) as a function of t_5 . (c) Schematic $U - J_H$ phase diagram for finite t_5 . Parameters are the same as those used in Fig. 1(d).

Acknowledgments—We thank K.-J. Yang, H.-M. Yi, M. Zeng, and C.-X. Liu for helpful discussions. We thank C. Lu for discussions and collaborations on closely related projects. L. H. H. is supported by National Key R&D Program of China (Grant No. 2022YFA1402200), the National Natural Science Foundation of China (Grant No. 12034017). Z. M. W. and D. H. X. were supported in part by the NSFC (Grants No. 12074108, No. 12474151, and No. 12347101), the Natural Science Foundation of Chongqing (Grant No. CSTB2022NSCQ-MSX0568). S. B. Z. acknowledges the support of the start-up fund at Hefei National Laboratory, the Innovation Program for Quantum Science and Technology (Grant No. 2021ZD0302800), and the National Natural Science Foundation of China (Grant No. 12488101). Z. M. W. and L. H. H. is supported by the start-up of Zhejiang University and the Fundamental Research Funds for the Central Universities (Grant No. 226-2024-00068).

L. H. H. initiated the idea and led the project. Y. Z., S. B. Z., and D. H. X. contributed to the development of the idea. Z. M. W., Y. Z., and L. H. H. performed the calculations with assistance from S. B. Z. and D. H. X. L. H. H., Y. Z., S. B. Z., and E. D. wrote the manuscript with input from all authors.

-
- [1] Y. Tokura and N. Nagaosa, Orbital physics in transition-metal oxides, *Science* **288**, 462 (2000).
- [2] J. A. Sobota, Y. He, and Z.-X. Shen, Angle-resolved photoemission studies of quantum materials, *Rev. Mod. Phys.* **93**, 025006 (2021).
- [3] Y. Cao, J. Waugh, X. Zhang, J.-W. Luo, Q. Wang, T. Reber, S. Mo, Z. Xu, A. Yang, J. Schneeloch *et al.*, Mapping the orbital wavefunction of the surface states in three-dimensional topological insulators, *Nat. Phys.* **9**, 499 (2013).
- [4] H. Zhang, C.-X. Liu, and S.-C. Zhang, Spin-orbital texture in topological insulators, *Phys. Rev. Lett.* **111**, 066801 (2013).
- [5] Z.-H. Zhu, C. N. Veenstra, G. Levy, A. Ubaldini, P. Syers, N. P. Butch, J. Paglione, M. W. Haverkort, I. S. Elfimov, and A. Damascelli, Layer-by-layer entangled spin-orbital texture of the topological surface state in Bi_2Se_3 , *Phys. Rev. Lett.* **110**, 216401 (2013).
- [6] L. Šmejkal, R. González-Hernández, T. Jungwirth, and J. Sinova, Crystal time-reversal symmetry breaking and spontaneous Hall effect in collinear antiferromagnets, *Sci. Adv.* **6**, eaaz8809 (2020).
- [7] M. Naka, S. Hayami, H. Kusunose, Y. Yanagi, Y. Motome, and H. Seo, Spin current generation in organic antiferromagnets, *Nat. Commun.* **10**, 4305 (2019).
- [8] K.-H. Ahn, A. Hariki, K.-W. Lee, and J. Kuneš, Antiferromagnetism in RuO_2 as d -wave pomeranchuk instability, *Phys. Rev. B* **99**, 184432 (2019).
- [9] S. Hayami, Y. Yanagi, and H. Kusunose, Momentum-dependent spin splitting by collinear antiferromagnetic ordering, *J. Phys. Soc. Jpn.* **88**, 123702 (2019).
- [10] L.-D. Yuan, Z. Wang, J.-W. Luo, E. I. Rashba, and A. Zunger, Giant momentum-dependent spin splitting in centrosymmetric low- z antiferromagnets, *Phys. Rev. B* **102**, 014422 (2020).
- [11] I. I. Mazin, K. Koepf, M. D. Johannes, R. González-Hernández, and L. Šmejkal, Prediction of unconventional magnetism in doped FeSb_2 , *Proc. Natl. Acad. Sci. U.S.A.* **118**, e2108924118 (2021).
- [12] H.-Y. Ma, M. Hu, N. Li, J. Liu, W. Yao, J.-F. Jia, and J. Liu, Multifunctional antiferromagnetic materials with giant piezomagnetism and noncollinear spin current, *Nat. Commun.* **12**, 2846 (2021).
- [13] L. Šmejkal, J. Sinova, and T. Jungwirth, Beyond conventional ferromagnetism and antiferromagnetism: A phase with nonrelativistic spin and crystal rotation symmetry, *Phys. Rev. X* **12**, 031042 (2022).
- [14] L. Šmejkal, J. Sinova, and T. Jungwirth, Emerging research landscape of altermagnetism, *Phys. Rev. X* **12**, 040501 (2022).
- [15] J. Krempaský, L. Šmejkal, S. D'souza, M. Hajlaoui, G. Springholz, K. Uhlířová, F. Alarab, P. Constantinou, V. Strocov, D. Usanov *et al.*, Altermagnetic lifting of Kramers spin degeneracy, *Nature (London)* **626**, 517 (2024).
- [16] H. Li, G. Wang, N. Ding, Q. Ren, G. Zhao, W. Lin, J. Yang, W. Yan, Q. Li, R. Yang, S. Yuan, J. D. Denlinger, Z. Wang, X. Zhang, L. A. Wray, S. Dong, D. Qian, and L. Miao, Spectroscopic evidence of spin-state excitation in d -electron correlated semiconductor FeSb_2 , *Proc. Natl. Acad. Sci. U.S.A.* **121**, e2321193121 (2024).
- [17] T. Jungwirth, R. M. Fernandes, J. Sinova, and L. Šmejkal, Altermagnets and beyond: Nodal magnetically-ordered phases, [arXiv:2409.10034](https://arxiv.org/abs/2409.10034).
- [18] L. Bai, W. Feng, S. Liu, L. Šmejkal, Y. Mokrousov, and Y. Yao, Altermagnetism: Exploring new frontiers in magnetism and spintronics, *Adv. Funct. Mater.* **34**, 2409327 (2024).
- [19] S. S. Fender, O. Gonzalez, and D. K. Bediako, Altermagnetism: A chemical perspective, *J. Am. Chem. Soc.* **147**, 2257 (2025).
- [20] Q. Liu, X. Dai, and S. Blügel, Different facets of unconventional magnetism, *Nat. Phys.* **21**, 329 (2025).
- [21] O. Fedchenko, J. Minár, A. Akashdeep, S. W. D'Souza, D. Vasilyev, O. Tkach, L. Odenbreit, Q. Nguyen, D. Kutnyakhov, N. Wind *et al.*, Observation of time-reversal symmetry breaking in the band structure of altermagnetic RuO_2 , *Sci. Adv.* **10**, eadj4883 (2024).
- [22] Z. Lin, D. Chen, W. Lu, X. Liang, S. Feng, K. Yamagami, J. Osiecki, M. Leandersson, B. Thiagarajan, J. Liu *et al.*, Observation of giant spin splitting and d -wave spin texture in room temperature altermagnet RuO_2 , [arXiv:2402.04995](https://arxiv.org/abs/2402.04995).
- [23] R. Gonzalez Betancourt, J. Zubáč, R. Gonzalez-Hernandez, K. Geishendorf, Z. Šobáň, G. Springholz, K. Olejník, L. Šmejkal, J. Sinova, T. Jungwirth *et al.*, Spontaneous anomalous Hall effect arising from an unconventional compensated magnetic phase in a semiconductor, *Phys. Rev. Lett.* **130**, 036702 (2023).
- [24] J. Krempaský, L. Šmejkal, S. D'souza, M. Hajlaoui, G. Springholz, K. Uhlířová, F. Alarab, P. Constantinou, V. Strocov, D. Usanov *et al.*, Altermagnetic lifting of Kramers spin degeneracy, *Nature (London)* **626**, 517 (2024).

- [25] S. Lee, S. Lee, S. Jung, J. Jung, D. Kim, Y. Lee, B. Seok, J. Kim, B. G. Park, L. Šmejkal *et al.*, Broken Kramers degeneracy in altermagnetic MnTe, *Phys. Rev. Lett.* **132**, 036702 (2024).
- [26] T. Osumi, S. Souma, T. Aoyama, K. Yamauchi, A. Honma, K. Nakayama, T. Takahashi, K. Ohgushi, and T. Sato, Observation of a giant band splitting in altermagnetic MnTe, *Phys. Rev. B* **109**, 115102 (2024).
- [27] Z. Liu, M. Ozeki, S. Asai, S. Itoh, and T. Masuda, Chiral split magnon in altermagnetic MnTe, *Phys. Rev. Lett.* **133**, 156702 (2024).
- [28] S. Reimers, L. Odenbreit, L. Šmejkal, V. N. Strocov, P. Constantinou, A. B. Hellenes, R. Jaeschke Ubierno, W. H. Campos, V. K. Bharadwaj, A. Chakraborty *et al.*, Direct observation of altermagnetic band splitting in CrSb thin films, *Nat. Commun.* **15**, 2116 (2024).
- [29] J. Ding, Z. Jiang, X. Chen, Z. Tao, Z. Liu, T. Li, J. Liu, J. Sun, J. Cheng, J. Liu *et al.*, Large band splitting in g-wave altermagnet CrSb, *Phys. Rev. Lett.* **133**, 206401 (2024).
- [30] G. Yang, Z. Li, S. Yang, J. Li, H. Zheng, W. Zhu, Z. Pan, Y. Xu, S. Cao, W. Zhao *et al.*, Three-dimensional mapping of the altermagnetic spin splitting in CrSb, *Nat. Commun.* **16**, 1442 (2025).
- [31] B. Jiang, M. Hu, J. Bai, Z. Song, C. Mu, G. Qu, W. Li, W. Zhu, H. Pi, Z. Wei *et al.*, A metallic room-temperature d-wave altermagnet, *Nat. Phys.* **21**, 754 (2025).
- [32] F. Zhang, X. Cheng, Z. Yin, C. Liu, L. Deng, Y. Qiao, Z. Shi, S. Zhang, J. Lin, Z. Liu *et al.*, Crystal-symmetry-paired spin–valley locking in a layered room-temperature metallic altermagnet candidate, *Nat. Phys.* **21**, 760 (2025).
- [33] J. E. Hirsch, Spin-split states in metals, *Phys. Rev. B* **41**, 6820 (1990).
- [34] C. Wu and S.-C. Zhang, Dynamic generation of spin-orbit coupling, *Phys. Rev. Lett.* **93**, 036403 (2004).
- [35] C. Wu, K. Sun, E. Fradkin, and S.-C. Zhang, Fermi liquid instabilities in the spin channel, *Phys. Rev. B* **75**, 115103 (2007).
- [36] H. Ikeda and Y. Ohashi, Theory of unconventional spin density wave: A possible mechanism of the micromagnetism in u-based heavy fermion compounds, *Phys. Rev. Lett.* **81**, 3723 (1998).
- [37] H. Chen, Q. Niu, and A. H. MacDonald, Anomalous Hall effect arising from noncollinear antiferromagnetism, *Phys. Rev. Lett.* **112**, 017205 (2014).
- [38] S. Nakatsuji, N. Kiyohara, and T. Higo, Large anomalous Hall effect in a non-collinear antiferromagnet at room temperature, *Nature (London)* **527**, 212 (2015).
- [39] L. Šmejkal, A. H. MacDonald, J. Sinova, S. Nakatsuji, and T. Jungwirth, Anomalous Hall antiferromagnets, *Nat. Rev. Mater.* **7**, 482 (2022).
- [40] J. Ren, X. Chen, Y. Zhu, Y. Yu, A. Zhang, J. Li, C. Li, and Q. Liu, Enumeration and representation of spin space groups, [arXiv:2307.10369](https://arxiv.org/abs/2307.10369).
- [41] Y. Jiang, Z. Song, T. Zhu, Z. Fang, H. Weng, Z.-X. Liu, J. Yang, and C. Fang, Enumeration of spin-space groups: Towards a complete description of symmetries of magnetic orders, [arXiv:2307.10371](https://arxiv.org/abs/2307.10371).
- [42] Z. Xiao, J. Zhao, Y. Li, R. Shindou, and Z.-D. Song, Spin space groups: Full classification and applications, [arXiv:2307.10364](https://arxiv.org/abs/2307.10364).
- [43] E. Liu, Y. Sun, N. Kumar, L. Muechler, A. Sun, L. Jiao, S.-Y. Yang, D. Liu, A. Liang, Q. Xu *et al.*, Giant anomalous Hall effect in a ferromagnetic kagome-lattice semimetal, *Nat. Phys.* **14**, 1125 (2018).
- [44] Y.-P. Zhu, X. Chen, X.-R. Liu, Y. Liu, P. Liu, H. Zha, G. Qu, C. Hong, J. Li, Z. Jiang *et al.*, Observation of plaid-like spin splitting in a noncoplanar antiferromagnet, *Nature (London)* **626**, 523 (2024).
- [45] M. Naka, Y. Motome, and H. Seo, Perovskite as a spin current generator, *Phys. Rev. B* **103**, 125114 (2021).
- [46] D.-F. Shao, S.-H. Zhang, M. Li, C.-B. Eom, and E. Y. Tsymbal, Spin-neutral currents for spintronics, *Nat. Commun.* **12**, 7061 (2021).
- [47] Z. Feng, X. Zhou, L. Šmejkal, L. Wu, Z. Zhu, H. Guo, R. González-Hernández, X. Wang, H. Yan, P. Qin *et al.*, An anomalous Hall effect in altermagnetic ruthenium dioxide, *Natl. Electron. Rev.* **5**, 735 (2022).
- [48] R. M. Fernandes, V. S. de Carvalho, T. Birol, and R. G. Pereira, Topological transition from nodal to nodeless Zeeman splitting in altermagnets, *Phys. Rev. B* **109**, 024404 (2024).
- [49] R.-W. Zhang, C. Cui, R. Li, J. Duan, L. Li, Z.-M. Yu, and Y. Yao, Predictable gate-field control of spin in altermagnets with spin-layer coupling, *Phys. Rev. Lett.* **133**, 056401 (2024).
- [50] R. He, D. Wang, N. Luo, J. Zeng, K.-Q. Chen, and L.-M. Tang, Nonrelativistic spin-momentum coupling in antiferromagnetic twisted bilayers, *Phys. Rev. Lett.* **130**, 046401 (2023).
- [51] S. Bhowal and N. A. Spaldin, Ferroically ordered magnetic octupoles in d-wave altermagnets, *Phys. Rev. X* **14**, 011019 (2024).
- [52] V. Leeb, A. Mook, L. Šmejkal, and J. Knolle, Spontaneous formation of altermagnetism from orbital ordering, *Phys. Rev. Lett.* **132**, 236701 (2024).
- [53] P. Das, V. Leeb, J. Knolle, and M. Knap, Realizing altermagnetism in Fermi-Hubbard models with ultracold atoms, *Phys. Rev. Lett.* **132**, 263402 (2024).
- [54] A. Chakraborty, R. González Hernández, L. Šmejkal, and J. Sinova, Strain-induced phase transition from antiferromagnet to altermagnet, *Phys. Rev. B* **109**, 144421 (2024).
- [55] L. Šmejkal, Altermagnetic multiferroics and altermagneto-electric effect, [arXiv:2411.19928](https://arxiv.org/abs/2411.19928).
- [56] X. Duan, J. Zhang, Z. Zhu, Y. Liu, Z. Zhang, I. Žutić, and T. Zhou, Antiferroelectric altermagnets: Antiferroelectricity alters magnets, *Phys. Rev. Lett.* **134**, 106801 (2025).
- [57] M. Gu, Y. Liu, H. Zhu, K. Yananose, X. Chen, Y. Hu, A. Stroppa, and Q. Liu, Ferroelectric switchable altermagnetism, *Phys. Rev. Lett.* **134**, 106802 (2025).
- [58] Z. Zhu, X. Duan, J. Zhang, B. Hao, I. Zutic, and T. Zhou, Two-dimensional ferroelectric altermagnets: From model to material realization, *Nano Lett.* **25**, 9456 (2025).
- [59] In the Sec. I of the SM [61], we additionally employ conventional magnetic space group notation to represent these symmetries: $\mathcal{P}_{A\leftrightarrow B}\mathcal{T}$, $\mathcal{C}_{4z}(X)\mathcal{T}$ and $\mathcal{M}_{A\leftrightarrow B}\mathcal{T}$. Importantly, in the absence of SOC, these symmetry operations

- maintain identical physical interpretations to the spin-space group symmetries.
- [60] P. Liu, J. Li, J. Han, X. Wan, and Q. Liu, Spin-group symmetry in magnetic materials with negligible spin-orbit coupling, *Phys. Rev. X* **12**, 021016 (2022).
- [61] See Supplemental Material at <http://link.aps.org/supplemental/10.1103/cjzw-j4v7> for tight-binding model details, Jahn-Teller distortion as a source of altermagnetism and spin conductivity, analytical nonrelativistic spin-orbital textures, anomalous Hall response, and the Ginzburg-Landau construction of spin-orbital altermagnetism, which includes Refs. [62–71].
- [62] T. A. Maier and S. Okamoto, Weak-coupling theory of neutron scattering as a probe of altermagnetism, *Phys. Rev. B* **108**, L100402 (2023).
- [63] A. S. Miñarro, M. Villa, B. Casals, S. Plana-Ruiz, F. Sánchez, J. Gázquez, and G. Herranz, Spin-orbit entanglement driven by the Jahn-Teller effect, *Nat. Commun.* **15**, 8694 (2024).
- [64] T. Moriya, *Spin Fluctuations in Itinerant Electron Magnetism* (Springer Science & Business Media, Berlin, 2012), Vol. 56.
- [65] F. Freimuth, S. Blügel, and Y. Mokrousov, Spin-orbit torques in Co/Pt(111) and Mn/W(001) magnetic bilayers from first principles, *Phys. Rev. B* **90**, 174423 (2014).
- [66] G. Kresse and J. Hafner, *Ab initio* molecular dynamics for liquid metals, *Phys. Rev. B* **47**, 558 (1993).
- [67] G. Kresse and J. Furthmüller, Efficient iterative schemes for *ab initio* total-energy calculations using a plane-wave basis set, *Phys. Rev. B* **54**, 11169 (1996).
- [68] P. E. Blöchl, Projector augmented-wave method, *Phys. Rev. B* **50**, 17953 (1994).
- [69] J. P. Perdew, K. Burke, and M. Ernzerhof, Generalized gradient approximation made simple, *Phys. Rev. Lett.* **77**, 3865 (1996).
- [70] S. L. Dudarev, G. A. Botton, S. Y. Savrasov, C. J. Humphreys, and A. P. Sutton, Electron-energy-loss spectra and the structural stability of nickel oxide: An LSDA + U study, *Phys. Rev. B* **57**, 1505 (1998).
- [71] Y. Yao, L. Kleinman, A. H. MacDonald, J. Sinova, T. Jungwirth, D.-s. Wang, E. Wang, and Q. Niu, First principles calculation of anomalous Hall conductivity in ferromagnetic bcc Fe, *Phys. Rev. Lett.* **92**, 037204 (2004).
- [72] R. González-Hernández, L. Šmejkal, K. Výborný, Y. Yahagi, J. Sinova, T. Jungwirth, and J. Železný, Efficient electrical spin splitter based on nonrelativistic collinear antiferromagnetism, *Phys. Rev. Lett.* **126**, 127701 (2021).
- [73] L. Šmejkal, A. B. Hellenes, R. González-Hernández, J. Sinova, and T. Jungwirth, Giant and tunneling magnetoresistance in unconventional collinear antiferromagnets with nonrelativistic spin-momentum coupling, *Phys. Rev. X* **12**, 011028 (2022).
- [74] A. Bose, N. J. Schreiber, R. Jain, D.-F. Shao, H. P. Nair, J. Sun, X. S. Zhang, D. A. Muller, E. Y. Tsybal, D. G. Schlom *et al.*, Tilted spin current generated by the collinear antiferromagnet ruthenium dioxide, *National electronics review* **5**, 267 (2022).
- [75] G. D. Mahan, *Many-Particle Physics* (Springer Science & Business Media, New York, 2013).
- [76] W. J. Kim, M. A. Smeaton, C. Jia, B. H. Goodge, B.-G. Cho, K. Lee, M. Osada, D. Jost, A. V. Ievlev, B. Moritz *et al.*, Geometric frustration of Jahn–Teller order in the infinite-layer lattice, *Nature (London)* **615**, 237 (2023).
- [77] Note that $\Delta p_s^n = 0$ in the \mathcal{O}_1 phase is valid only up to second-order perturbation, which is generally non-zero but negligible ($< 1\%$ relative to other phases) when computed using a complete tight-binding model (see the SM [61] for more details).
- [78] Note that in the absence of SOC, the Néel vector can point along any arbitrary direction.
- [79] I. Dzyaloshinsky, A thermodynamic theory of “weak” ferromagnetism of antiferromagnetics, *J. Phys. Chem. Solids* **4**, 241 (1958).
- [80] T. Moriya, Anisotropic superexchange interaction and weak ferromagnetism, *Phys. Rev.* **120**, 91 (1960).
- [81] C. Lu, C. Cao, H. Yuan, P. Coleman, and L.-H. Hu, Breakdown of stoner ferromagnetism by intrinsic altermagnetism, [arXiv:2510.00614](https://arxiv.org/abs/2510.00614).
- [82] M. Vila, V. Sunko, and J. E. Moore, Orbital-spin locking and its optical signatures in altermagnets, *Phys. Rev. B* **112**, L020401 (2025).
- [83] R. Jaeschke-Ubiergo, V.-K. Bharadwaj, W. Campos, R. Zarzuela, N. Biniskos, R. M. Fernandes, T. Jungwirth, J. Sinova, and L. Šmejkal, Atomic altermagnetism, [arXiv:2503.10797](https://arxiv.org/abs/2503.10797).
- [84] P. d’Ornellas, V. Leeb, A. G. Grushin, and J. Knolle, Altermagnetism without crystal symmetry, [arXiv:2504.08597](https://arxiv.org/abs/2504.08597).